Theoretical and Computational Acoustics
D. Lee, Y-H Pao, M.H. Schultz, and Y-C Teng (Editors)

Shallow Water Acoustic Propagation from an Embedded Source

G.D. Wills, C.L. Morfey, P.A. Nelson
Institute of Sound and Vibration Research, University of Southampton, U.K.

Abstract

The method of plane wave decomposition is used to model acoustic propagation in shallow water from a point source in the sea-bed. The work was prompted by the need to model blast waves emanating from explosive charges buried in boreholes, which are used to fragment unwanted bedrock. The water channel is assumed to be a homogeneous medium of constant depth, and a point spherical source is located below the rock-water boundary. By using the analytical decomposition of a spherical wave into plane wave components, the resulting pressure due to the spherical source is given as a single, one-dimensional integral. This integral is of a similar form to the well known expression for the case of a point source located within the water channel, and in fact the denominator is identical. Inverting the denominator as an infinite series produces a summation of integrals, or images, with each image corresponding to the exact pressure produced after a certain number of reflections from the water surface and sea-bed. The integrals are solved numerically using reliable adaptive integration routines and advanced computational power. It is not necessary to evaluate each individual image integral and then add them together, since the single integral that the image formulation converges to can be evaluated directly. By integrating the real and imaginary parts separately, results are produced for both the case of the point source in the sea-bed and the point source in the water. The effect of shear waves in the sea-bed is also incorporated into the model by using the fluid-solid plane wave reflection and transmission coefficients in the integrands. An experiment has been conducted to validate the results produced by the integration routine for the case of the point source within the water channel. This involved using a hydrophone as an impulsive source in a scale model shallow water channel of 12.5 cm depth, and measuring the propagation loss as a function of increasing radial distance. Excellent agreement was found between the measurements and the theoretical predictions. This paper presents details of the theoretical approach, and presents results in both the frequency and time domains. Comparison will then be made with the experimental results.

1 Introduction

Explosive charges buried in boreholes are used frequently in the underwater construction industry to fragment unwanted bed-rock. When the explosives are fired, the large pressure wave created in the water will radiate out and impinge upon any structures or swimmers/divers in the vicinity. A typical water depth involved is of the order of 10-30 metres.

Determining safe stand-off distances from the explosive site therefore calls for a study of transient propagation in shallow water from a source located in the sea-bed. The theoretical model being used is shown in Figure 1, in which a point spherical source is located at a depth of z_0 into a homogeneous elastic half space. The water channel is assumed to be a homogeneous medium of constant depth d. The receiver is located in the water channel at a height z above the sea-bed and at a radial distance r from the source. Due to the receiver and boundary often being situated well into the acoustic near-field of the source, models such as SAFARI would not produce accurate results for this propagation problem.

The theoretical formulation is identical to that used for the classic shallow water problem shown in Figure 2, where the source is located within the water channel. By decomposing the outgoing wave from the point spherical source into plane wave components, Brekovskikh [1] obtains an exact expression for the acoustic pressure in the latter case. After exploiting the circular symmetry using either Hankel or Bessel functions, the pressure in the water reduces to a single one-dimensional integral over the complex incident angle, θ_i; θ_i being the angle that each plane wave component makes with the z-axis. Two different analytical approaches have been used in the past to analyse the behaviour of the integrand. Firstly, the poles of the denominator correspond to the cut-on of modes within the shallow water channel. By deforming the path of integration in the complex θ_i plane, Brekovskikh uses Cauchy's method of residues to represent the acoustic field as a summation of normal modes. Zhang and Tindle[2], Glegg[3] and Chapman[4] then use approximate methods to characterise the most important features of the acoustic field.

The second analytical approach involves inverting the denominator as an infinite series to produce a summation of integrals, or images, with each image corresponding to the exact pressure produced after a certain number of reflections between the water surface and sea-bed. Various methods have been used to solve individual image integrals of this kind. Plumpton and Tindle [5] used saddle point analysis to calculate the field reflected back from a fluid-fluid interface. Westwood [6] allowed the angular dependent reflection coefficient to influence the location of the saddle points. Westwood was then able to calculate the pressure in flat and sloping shallow water waveguides by adding together such integrals [7].

For the point source in the sea-bed (Figure 1), the solution derived in the next section is found to be of a similar form to the single integral over complex angle given by Brekovskikh when the source is located in the water. Rather than taking either of the two above mentioned approximate methods to evaluate this integral, exact results are produced by direct numerical integration. By eliminating all poles in the integrand and using advanced computational power, it is possible to solve the single integral numerically in a reasonable amount of computation time. Even if a large number of modes are propagating, thus producing an extremely 'spiky' integrand, the numerical integration routine is still reliable. To demonstrate this, a comparison will be made between theoretical predictions and experiment for the case of the point source within the water channel.

2 Theoretical Solution for a Point Source in the Seabed

A point spherical source located in rock will generate only P waves, and hence the spherical wave generated by the source can be represented by the scalar displacement potential ϕ. Referring again to the geometry shown in Figure 1, and using the Sommerfeld integral [1] with a time dependence of $e^{j\omega t}$, the potential incident on the rock-water boundary ϕ_i is given by

$$\phi_i = \frac{e^{-jk_1\sqrt{r^2+z_0^2}}}{\sqrt{r^2+z_0^2}} = -jk_1 \int_\Gamma J_0\left(k_r r\right) e^{-jk_{z1}z_0} \sin\theta_i d\theta_i \tag{1}$$

where

$$k_r = k_1 \sin\theta_i \qquad k_{z1} = k_1 \cos\theta_i \qquad k_1 = \omega/c_p \tag{2}$$

and the path of integration Γ for the complex variable θ_i is shown in Figure 3.

The geometry has been reduced to plane wave propagation in the z-direction, with all radial dependence and circular symmetry being accounted for by the Bessel function. In order to arrive at an exact expression for the pressure in the water, a transfer function is now included in the Sommerfeld integrand of Equation (1). This transfer function must relate the plane wave components incident on the rock-water boundary to a point of interest within the shallow water channel. To arrive at this transfer function, consider firstly the case of no shear waves in the rock. By analysing the response of the three layer system shown in Figure 4, the transfer function will be given by

$$T\left(\theta_i, z\right) = \frac{\phi_2\left(z\right)}{\phi_i\left(\theta_i\right)} \tag{3}$$

where $\phi_2 = \phi_a + \phi_b$. Simple plane wave analysis yields

$$T\left(\theta_i, z\right) = \frac{T_1\left(e^{-jk_{z2}z} + R_2 e^{-jk_{z2}(2d-z)}\right)}{\left(1 - R_1 R_2 e^{-j2k_{z2}d}\right)} \tag{4}$$

where $T_1 = 2Z_1/\left(Z_1 + Z_2\right)$, the fluid-fluid plane wave transmission coefficient from the bottom into the water, $R_1 = \left(Z_1 - Z_2\right)/\left(Z_1 + Z_2\right)$, the fluid-fluid plane wave reflection coefficient seen from the water channel looking into the bottom, and $R_2 = \left(Z_3 - Z_2\right)/\left(Z_3 + Z_2\right)$, the fluid-fluid plane wave reflection coefficient seen from the water looking at the water surface, and where

$$Z_1 = \frac{\rho_1 c_p}{\cos\theta_i} \qquad Z_2 = \frac{\rho_2 c_2}{\cos\theta_2} \qquad Z_3 = \frac{\rho_3 c_3}{\cos\theta_3} \tag{5}$$

with

$$\frac{\sin\theta_i}{c_p} = \frac{\sin\theta_2}{c_2} = \frac{\sin\theta_3}{c_3}$$

Placing (4) into (1), the exact expression for the field in the water is given by

$$\phi = -jk_1 \int_\Gamma J_0\left(k_r r\right) e^{-jk_{z1}z_0} \frac{T_1\left(e^{-jk_{z2}z} + R_2 e^{-jk_{z2}(2d-z)}\right)}{\left(1 - R_1 R_2 e^{-j2k_{z2}d}\right)} \sin\theta_i d\theta_i \tag{6}$$

Equation (6) should now be compared to the exact expression arrived at by Brekovskikh for the field produced in the water when the source is also located in the water. For a point source of strength q and using the geometry shown in Figure 2, this is given by

$$p(r,z) = \frac{\omega\rho_1 q k_1}{4\pi}\int_\Gamma J_0(k_r r)\, e^{-jk_{z1}(z-z_0)}\frac{\left(1+R_1e^{-j2k_{z1}z_0}\right)\left(1+R_2e^{-j2k_{z1}(d-z)}\right)}{\left(1-R_1R_2e^{-j2k_{z1}d}\right)}\sin\theta_i d\theta_i \quad (7)$$

Note that the subscripts used to represent the bottom and water are interchanged in Figures 1 and 2, with the intention of making k_{z1} always represent the z-wavenumber in the same medium as the source. For a given z-wavenumber in the water channel, the denominators of equations (6) and (7) are therefore identical. From a modal standpoint this is reasonable, since the same poles are expected. Brekovskikh replaced the denominator by an infinite series, using the relation

$$\left(1-R_1R_2e^{-j2k_{z2}d}\right)^{-1} = \sum_{l=0}^{\infty}(R_1R_2)^l\, e^{-j2k_{z2}dl} \quad (8)$$

By applying equation (8) to the denominator of equation (6), the field in the water is written as

$$\phi = -jk_1\sum_{l=0}^{\infty}\int_\Gamma J_0(k_r r)\, e^{-jk_{z1}z_0}T_1\left(e^{-jk_{z2}(z+2dl)} + R_2e^{-jk_{z2}(2d(l+1)-z)}\right)(R_1R_2)^l\sin\theta_i d\theta_i \quad (9)$$

Equation (9) can now be interpreted as an image model. For example, when $l=0$, equation (9) is given by

$$\phi = -jk_1\int_\Gamma J_0(k_r r)\, e^{-j(k_{z1}z_0+k_{z2}z)}T_1\sin\theta_i d\theta_i - jk_1\int_\Gamma J_0(k_r r)\, e^{-j(k_{z1}z_0+k_{z2}(2d-z))}T_1R_2\sin\theta_i d\theta_i \quad (10)$$

The first integral in (10) is the exact field produced at a receiver position after transmitting through the lower boundary into the water as if the water surface was not present. The second integral is the exact field produced in the water due to the source transmitting through the boundary, reflecting off of the water surface, and transmitting back down to the same receiver position. Upon increasing l in (9), the number of reflections between the water surface and sea-bed progressively increases. With this image model in mind, it is clear that the expressions for T_1 and R_1 in equation (6) can be extended to the case of an elastic lower medium. Equation (6) would then be solved using the solid-fluid transmission coefficient and the fluid-solid reflection coefficient, given by

$$T_1 = \frac{2\rho_1 Z_2\cos 2\gamma}{\rho_2\left(Z_1\cos^2 2\gamma + Z_s\sin^2 2\gamma + Z_2\right)} \quad (11)$$

and

$$R_1 = \frac{\left(Z_1\cos^2 2\gamma + Z_s\sin^2 2\gamma - Z_2\right)}{\left(Z_1\cos^2 2\gamma + Z_s\sin^2 2\gamma + Z_2\right)} \quad (12)$$

where

$$Z_s = \frac{\rho_1 c_s}{\cos\gamma} \quad (13)$$

and

$$\frac{\sin\theta_i}{c_p} = \frac{\sin\gamma}{c_s}$$

The method used to solve these equations will now be discussed.

3 Computational Method

Rather than taking the modal approach, the complete integral expressions in the form of equations (6) and (7) are evaluated numerically. In theory, it is necessary to evaluate up to infinity along the evanescent path in Figure 3. In practice, it is sufficient to evaluate as far as a truncation value $\theta_i = \frac{\pi}{2} + ja_t$ where the value of a_t is determined by investigating the decay of the exponential terms in the integrand. Several tests were performed to check that the integral had converged, by progressively increasing the value of a_t.

Direct numerical integration is only possible if the integrand is in a form where there are no poles present, otherwise the adaptive integration routine will break down. This involves implementing the reflection and transmission coefficients in the form

$$R_1 = \frac{\cos^2 2\gamma/Z_2Z_s + \sin^2 2\gamma/Z_1Z_2 - 1/Z_1Z_s}{\cos^2 2\gamma/Z_2Z_s + \sin^2 2\gamma/Z_1Z_2 + 1/Z_1Z_s} \tag{14}$$

otherwise poles exist in the impedances Z_n at the point where the cosine of the associated angle equals zero. The only pole remaining in (14) corresponds to the Stoneley wave, and was eliminated by introducing a small imaginary part to the shear wave speed.

There is still one other point in equations (6) and (7) to be considered, which corresponds to plane waves within the water channel which travel at grazing incidence to the sea-bed. For both equations (6) and (7), the integrand takes a value of 0/0. L'Hopital's rule was used to calculate the limiting value at this point. For the case of the point source in the water, the limiting value is zero. For the case of the point source in the sea-bed, the limiting value is not zero, but the adaptive integration routine does not have any problems in following the smooth behaviour of the integrand around this point.

The image models serve as a useful means of checking the reliability of integrating equations (6) or (7) directly. The image integrals are much easier to integrate numerically, as they do not contain the spiky behaviour caused by the generation of modes. A comparison was made between the result obtained by adding together the summation of image integrals, and the result obtained by directly integrating either equations (6) and (7). The same answer is produced, though integrating equations (6) and (7) directly takes a considerably smaller amount of computation time.

Time domain results are produced by evaluating equations (6) or (7) at discrete frequencies over a band of interest, followed by an inverse FFT. The response to any source time history can then be found by convolution.

4 Results and Comparison with Experiment

An experiment was conducted to test the results produced by the numerical integration routine. This involved using a hydrophone as a point source in a scale model shallow water

channel of 12.5 cm depth. The parameters of the base of the channel were determined by obtaining data from the manufacturers for the elastic parameters of the particular type of concrete used, from which the compressional wave and shear wave speed were calculated. The propagation loss as a function of range was measured for several specific values of z_0 and z, and then compared to the theoretical results obtained by directly evaluating equation (7). Figure 5 shows the propagation loss at two different ratios of acoustic wavelength in water λ to the water depth d. Good agreement was observed between experiment and theory.

A time domain comparison was also made between experiment and theory. This was achieved by firstly determining the bandwidth over which it is possible to get good agreement in the frequency domain, and then using the same bandwidth in the theoretical calculations. Two time domain comparisons are shown in Figure 6. The ringing of the impulsive output from the hydrophone has been deconvolved out as far as possible by the use of an inverse filter. Figure 7 shows a theoretical prediction when the source is located in the rock. In order to get good resolution in the time domain, a relatively large bandwidth was used. The source time history used in the top diagram of Figure 7 is a Hanning pulse. The first arrival corresponds to a ray path travelling through the rock and then refracted up in the water to the receiver position. Later arrivals correspond to the ray paths of the images. The relatively low frequency arrival is due to evanescent energy incident on the rock-water boundary. The lower plot in Figure 7 shows the result of effectively filtering out the evanescent waves incident on the rock-water boundary by modifying the incident pulse waveform to remove the low-frequency energy, and thus ensuring that the boundary is in the far-field of all of the impulsive energy produced by the source. The low frequency arrival can be seen to be removed.

5 Conclusions

The mathematical formulation of an image model has been arrived at for the case of a point source located in the sea-bed. It is not necessary to evaluate each individual image integral separately followed by summation, as the single integral that the result converges to can be evaluated directly. Exact results have been produced using this numerical integration technique for both the case of the point source in the sea-bed and the point source in the water, though this is only possible in a reasonable amount of computation time using advanced computational power. A typical amount of time taken is 7 minutes for a 2048 point spectrum running on a Silicon Graphics Indigo Elan/R4000 workstation.

References

[1] L.M. Brekovskikh, '*Waves in Layered Media*' Academic Press, New York 2nd Ed.

[2] Z.Y. Zhang and C.T. Tindle, 'Complex effective depth of the ocean bottom', *J.Acoust. Soc. Am.* **93**, 205-213 (1993).

[3] S.A.L. Glegg, 'The effective depth approximation for sound propagation in shallow water over a sediment layer and a hard rock basement', *J.Acoust. Soc. Am.* **94**, 3302-3311 (1993)

[4] D.M.F Chapman, P.D. Ward and D.D. Ellis, 'The effective depth of a Pekeris ocean waveguide including shear wave effects', *J.Acoust. Soc. Am.* **85**, 648-653 (1989)

[5] N.G. Plumpton and C.T. Tindle, 'Saddle point analysis of the reflected acoustic field', *J.Acoust. Soc. Am.* **85** 1115-1123 (1989)

[6] E.K. Westwood, 'Complex ray methods for acoustic interaction at a fluid-fluid interface', *J.Acoust. Soc. Am.* **85** 1872-1884 (1989)

[7] E.K. Westwood, 'Ray methods for flat and sloping shallow water waveguides', *J.Acoust. Soc. Am.* **85** 1885-1894 (1989)

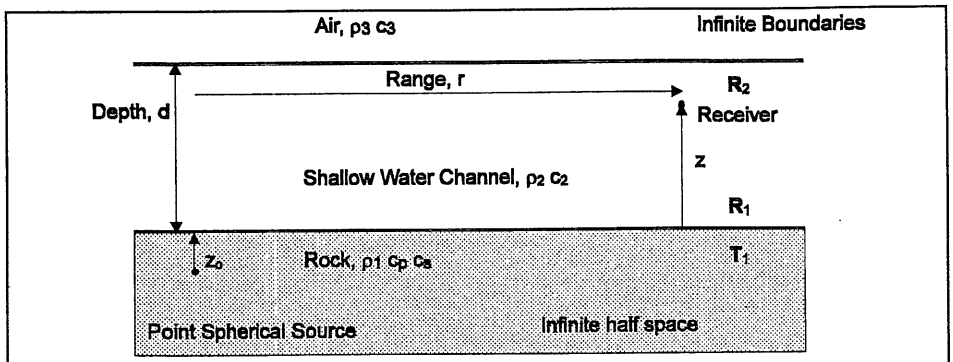

Figure 1 *The theoretical model being used to study shallow water propagation from an embedded source. The water channel is assumed to be a homogeneous medium of constant depth d.*

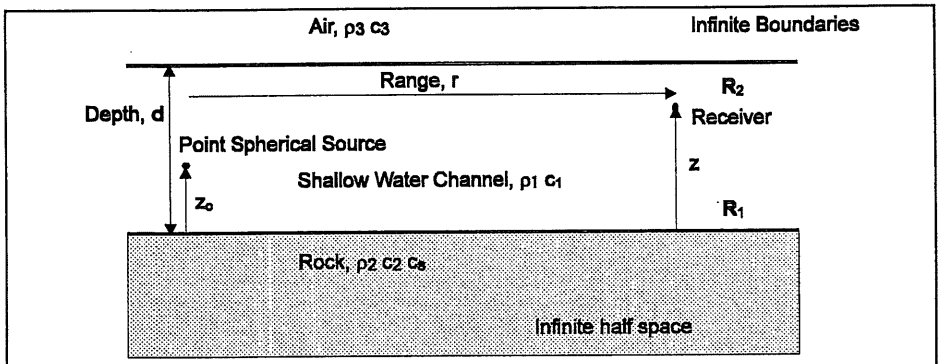

Figure 2 *Geometry used in which the source is located within the shallow water channel*

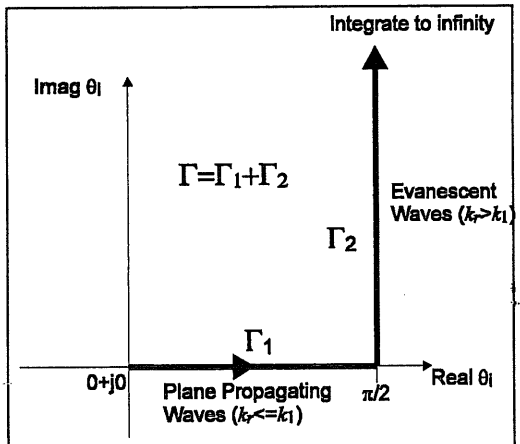

Figure 3 *The path of integration of the complex angle* θ_i

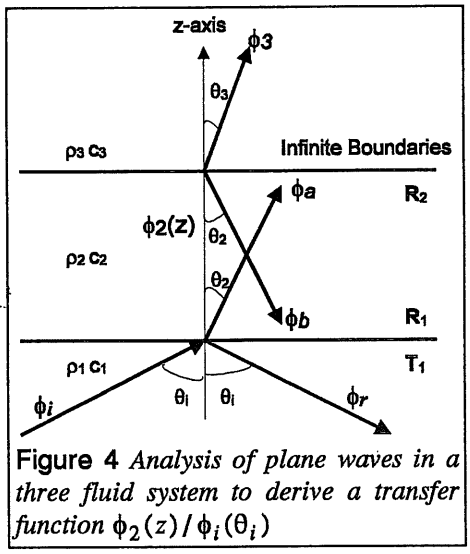

Figure 4 *Analysis of plane waves in a three fluid system to derive a transfer function* $\phi_2(z)/\phi_i(\theta_i)$

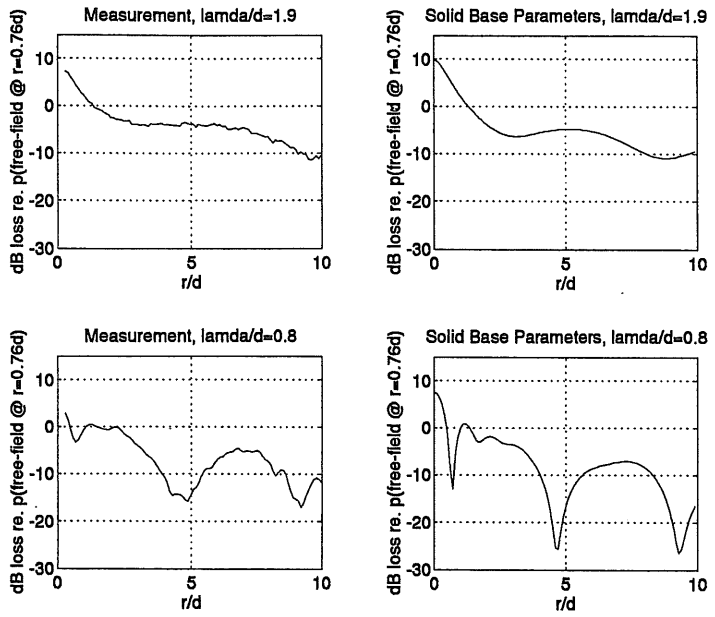

Figure 5 *Theoretical and experimental propagation loss for a point source within the shallow water channel at two different ratios of* λ/d $(z_0 / d = 0.5$ *and* $z / d = 0.12)$.

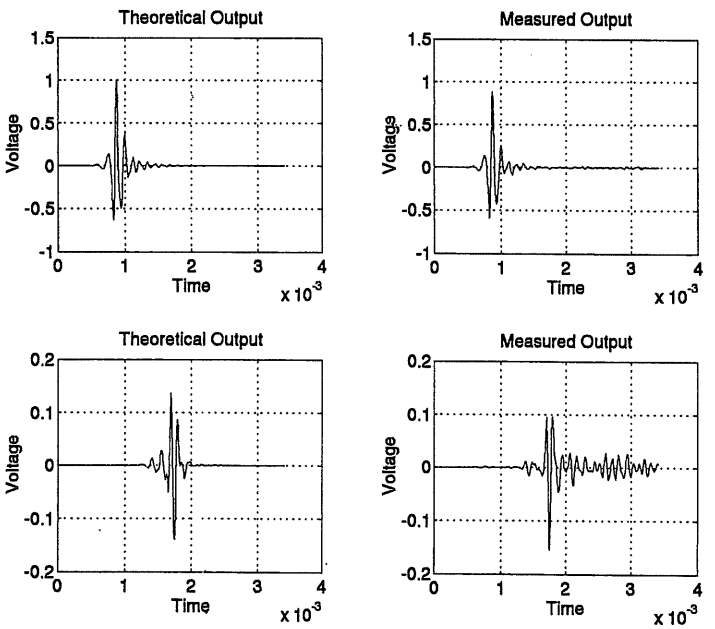

Figure 6 *Theoretical and experimental pulse propagation for a point source within the shallow water channel at two specific receiver positions (both with* $z_0 / d = 0.5$ *and* $z / d = 0.12$*). The first position is very close to the source* $(r / d = 0.3)$*. The second position is at* $r / d = 10$*, where the presence of head waves can be clearly seen in both the theory and experiment. The later arrivals in the measurement are side reflections from the experimental tank.*

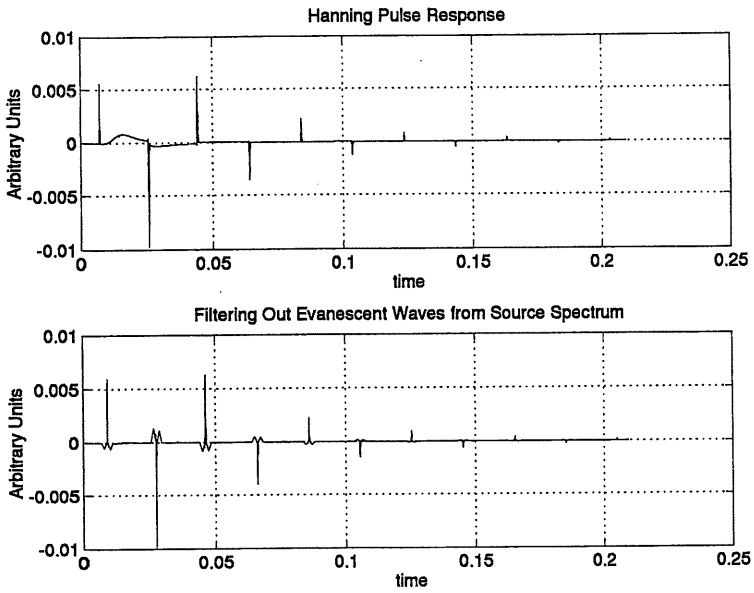

Figure 7 *Theoretical Hanning pulse response in shallow water from a point source in the sea-bed, and the result of filtering out the evanescent field incident on the rock-water boundary. The parameters used are* $z_0 = 10\,\mathrm{m}$ $r = 20\,\mathrm{m}$ $z = 0.1\,\mathrm{m}$ $d = 15\,\mathrm{m}$ ρ_1=2600kg/m^3 ρ_2=1000kg/m^3 ρ_3=1.2kg/m^3 $c_p = 3700\,\mathrm{m/s}$ c_s=(2200+j)m/s c_2=1500m/s c_3=344m/s.